Decoupled Homography-based Visual Servoing with Omnidirectional Cameras

Hicham Hadj-Abdelkader, Youcef Mezouar, Nicolas Andreff and Philippe Martinet
LASMEA, 24 avenue des Landais - 63177 Aubiere Cedex, France
Email: {hadj,mezouar,andreff,martinet}@lasmea.univ-bpclermont.fr

***Abstract*— This paper presents a new hybrid decoupled vision-based control scheme valid for the entire class of central catadioptric sensors (including conventional perspective cameras). First, we consider the structure from motion problem using imaged 3D lines (conics). Polar lines of the principal point with respect to the conic curves are exploited to estimate a generic homography matrix from which a partial Euclidean reconstruction is obtained. The polar lines and the information extracted from the homography are then used to design a control law which allow us to fully decouple rotational motions from translational motions.**

I. Introduction

Vision-based servoing schemes are flexible and effective methods to control robot motion from camera observations. They are generally classified into three groups, namely position-based, image-based and hybrid-based control [13], [16]. These three schemes make assumptions on the link between the initial, current and desired images since they require correspondences between the visual features extracted from the initial image with those obtained from the desired one. These features are then tracked during the camera (and/or the object) motion. If these steps fail the visually based robotic task can not be achieved [7]. Typical cases of failure arise when matching joint image features is impossible (for example when no joint feature belongs to initial and desired images) or when some parts of the image features get out of the field of view during the servoing. Some methods were investigated to resolve this deficiency based on path planning [17], switching control [8], zoom adjustment [20], geometrical and topological considerations [9]. However, such strategies are sometimes delicate to adapt to a generic setup. Conventional cameras suffer thus from restricted field of view. There is thus significant motivation for increasing the field of view of the cameras [5]. Many applications in vision-based robotics, such as mobile robot localization [6] and navigation [22], can benefit from the panoramic field of view provided by omnidirectional cameras. In the literature, there have been several methods proposed for increasing the field of view of cameras systems [5]. One effective way is to combine mirrors with conventional imaging system. The obtained sensors are referred to as catadioptric imaging systems. The resulting imaging systems have been termed central catadioptric when a single projection center describes the world to image mapping. From a theoretical and practical view point, a single center of projection is a desirable property for an imaging system [2]. Baker and Nayar in [2] derive the entire class of catadioptric systems with a single viewpoint. Clearly, visual servoing applications can also benefit from such sensors since the latter naturally overcome the visibility constraint. Vision-based control of robotic arms, single mobile robot or formation of mobile robots appear thus in the literature with omnidirectional cameras (refer for example to [4], [19], [21],[18]). Image-based visual servoing with central catadioptric cameras using points was studied in [4]. The use of straight lines has also been investigated in [18]. As it is well known, the catadioptric projection of a 3D line in the image plane is a conic curve. In [18], the authors propose to use directly the coordinates of the polar lines of the image center with respect to the conic curves to define the input of the vision-based control scheme.

This paper is concerned with homography-based visual servo control techniques with central catadioptric cameras. This framework, also called 2 1/2 D visual servoing [16] in the case where the image features are points, exploits a combination of reconstructed Euclidean information and image features in the control design. The 3D information is extracted from an homography matrix relating two views of a reference plane. As a consequence, the 2 1/2 D visual servoing scheme does not require any 3D model of the target. Unfortunately, in such approach when conventional cameras are used, the image of the target is not guaranteed to remain in the camera field of view. To overcome this deficiency 2 1/2 D visual servoing has been extented to an entire class of omnidirectional cameras in [12]. The resulting interaction matrices are triangular with partial decoupling properties (refer to [16], [12]).

In this paper a new approach for homography-based visual servoing using 3D-lines imaged with any type of central camera is presented. The structure from motion problem using imaged 3D co-planar lines (conics) is first studied. Geometrical relationship between polar lines and conic curves are exploited to linearly estimate a generic homagraphy matrix from which a partial Euclidean reconstruction is obtained. The polar lines and the information extracted from the homography are then used to design a control law which allow us to fully decouple rotational motions from translational motions (*i.e* the resulting interaction matrix is square block-diagonal).

II. Modelisation

A. Central catadioptric camera model

The catadioptric projection can be modeled by a central projection onto a virtual unitary sphere, followed by a perspective

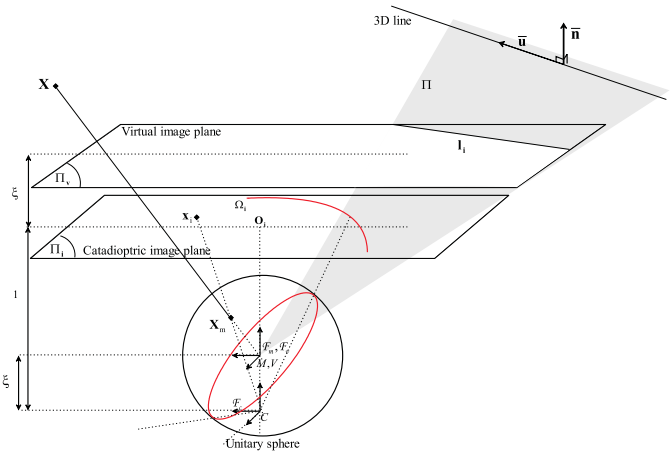

Fig. 1. Central catadioptric image formation

projection onto an image plane. This virtual unitary sphere is centered in the principal effective view point and the image plane is attached to the perspective camera.

As shown in figure 1, $\mathcal{F}_c$ and $\mathcal{F}_m$ are the frames attached to the conventional camera and to the mirror respectively. In the sequel, we assume that $\mathcal{F}_c$ and $\mathcal{F}_m$ have the same orientation. The origins C and M of $\mathcal{F}_c$ and $\mathcal{F}_m$ will be termed optical center and principal projection center respectively. The optical center C has coordinates $[0\ 0\ -\xi]^T$ with respect to $\mathcal{F}_m$ and the image plane $Z = 1-\xi$ is orthogonal to the Z-axis where ξ and ψ describe the type of sensor and the shape of the mirror, and are function of mirror shape parameters (refer to [3]).

1) Projection of points: Let $\mathcal{X}$ be a 3D point with coordinates $\mathbf{X} = [X\ Y\ Z]^T$ with respect to $\mathcal{F}_m$. The world point $\mathcal{X}$ is imaged in the image plane into the point of homogeneous coordinates $\mathbf{x} = [x\ y\ 1]^T$.

$$\mathbf{x} = \mathbf{K}\left[\frac{X}{Z+\xi\|\mathbf{X}\|}\ \ \frac{Y}{Z+\xi\|\mathbf{X}\|}\ \ 1\right]^T \tag{1}$$

The matrix $\mathbf{K}$ can be written as $\mathbf{K} = \mathbf{K_c}\mathbf{M}$ where the upper triangular matrix $\mathbf{K_c}$ contains the conventional camera intrinsic parameters, and the diagonal matrix $\mathbf{M}$ contains the mirror intrinsic parameters. Note that, setting $\xi = 0$, the general projection model becomes the well known perspective projection model.

2) Projection of lines: Let $\mathcal{L}$ be a 3D straight line in space lying on the interpretation plane which contains the principal projection center M (see Figure 1). The binormalized Euclidean Plücker coordinates [1] of the 3D line are defined as $\begin{bmatrix}\bar{\mathbf{u}}^T & \bar{\mathbf{h}}^T & h\end{bmatrix}^T$. The unit vectors $\bar{\mathbf{h}} = (h_x, h_y, h_z)^T$ and $\bar{\mathbf{u}} = (u_x, u_y, u_z)^T$ are respectively the orthogonal vector to the interpretation plane and the orientation of the 3D line $\mathcal{L}$ and are expressed in the mirror frame $\mathcal{F}_m$. h is the orthogonal distance from $\mathcal{L}$ to the origin of the definition frame. The unit vectors $\bar{\mathbf{h}}$ and $\bar{\mathbf{u}}$ are orthogonal, thus verifie $\bar{\mathbf{h}}^T\bar{\mathbf{u}} = 0$. If the 3D line is imaged by a perspective camera then the unit vector $\bar{\mathbf{h}}$ contains the coefficient of the 2D line $\mathbf{l}$ in the image plane (expressed in pixels), i.e the homogeneous coordinates $\mathbf{x}$ of the perspective projection of any world point lying on $\mathcal{L}$ verifies:

$$(\mathbf{K}^{-T}\bar{\mathbf{h}})^T\mathbf{x} = \mathbf{l}^T\mathbf{x} = 0 \tag{2}$$

with $\mathbf{l} = \mathbf{K}^{-T}\bar{\mathbf{h}}$. If the line is imaged with a central catadioptric camera then the 3D points on the 3D line $\mathcal{L}$ are mapped into points $\mathbf{x}$ lying on a conic curve in the catadioptric image:

$$\mathbf{x}^T\mathbf{K}^{-T}\mathbf{\Omega}\mathbf{K}^{-1}\mathbf{x} = \mathbf{x}^T\mathbf{\Omega_i}\mathbf{x} = 0 \tag{3}$$

where $\mathbf{\Omega}_i = \mathbf{K}^{-T}\mathbf{\Omega}\mathbf{K}^{-1}$ and:

$$\mathbf{\Omega} \propto \begin{bmatrix} h_x^2-\xi^2(1-h_y^2) & h_xh_y(1-\xi^2) & h_xh_z \\ h_xh_y(1-\xi^2) & h_y^2-\xi^2(1-h_x^2) & h_yh_z \\ h_xh_z & h_yh_z & h_z^2 \end{bmatrix}$$

B. Polar lines

The quadratic equation (3) is defined by five coefficients since $\mathbf{\Omega_i}$ is symmetric and defined up to scale factor. Nevertheless, the catadioptric image of a 3D line has only two degrees of freedom those of the interpretation plane definition. In the sequel, we show how we can get a minimal representation using polar lines.

Let Φ, A be respectively a 2D conic curve, a point in the definition plane of Φ. The polar line $\mathbf{l}$ of A with respect to Φ is defined by $\mathbf{l} \propto \Phi A$. Now, consider the principal point $\mathbf{O_i} = [u_0\ v_0\ 1]^T = \mathbf{K}[0\ 0\ 1]^T$ and the polar line $\mathbf{l}_i$ of $\mathbf{O_i}$ with respect to $\mathbf{\Omega_i}$: $\mathbf{l_i} \propto \mathbf{\Omega_i}\mathbf{O_i}$, then:

$$\begin{array}{rcl} \mathbf{l_i} & \propto & \mathbf{K}^{-T}\mathbf{\Omega}\mathbf{K}^{-1}\mathbf{O_i} = \mathbf{K}^{-T}\mathbf{\Omega}\mathbf{K}^{-1}\mathbf{K}[0\ 0\ 1]^T \\ & \propto & \mathbf{K}^{-T}\bar{\mathbf{h}} \end{array} \tag{4}$$

Moreover, equation (4) yields:

$$\bar{\mathbf{h}} = \frac{\mathbf{K}^\top\mathbf{l_i}}{\|\mathbf{K}^\top\mathbf{l_i}\|} \tag{5}$$

It is thus clear that the polar line $\mathbf{l_i}$ contains the coordinates of the projection of the 3D line $\mathcal{L}$ in an image plane of an equivalent (virtual) perspective camera defined by the frame $\mathcal{F}_v = \mathcal{F}_m$ (see figure 2) with internal parameters chosen equal to the internal parameters of the catadioptric camera (*i.e* $\mathbf{K_v} = \mathbf{K_c}\mathbf{M}$). This result is fundamental since it allows us to represent the physical projection of a 3D line in a catadioptric camera by a simple (polar) line in a virtual perspective camera rather than a conic. Knowing only the optical center $\mathbf{O_i}$, it is thus possible to use the linear pin-hole model for the projection of a 3D line instead of the non linear central catadioptric projection model.

In the sequel, we show how the homography related to a reference plane can be computed using polar lines and how it can be exploited to design a new vision-based control scheme which allows to fully decouple rotational and translational motions.

III. Scaled Euclidean Reconstruction Using Homography

The Euclidean reconstruction from two views is a non-linear problem. Several methods were proposed to solve this problem [10]. They are generally based on the estimation of

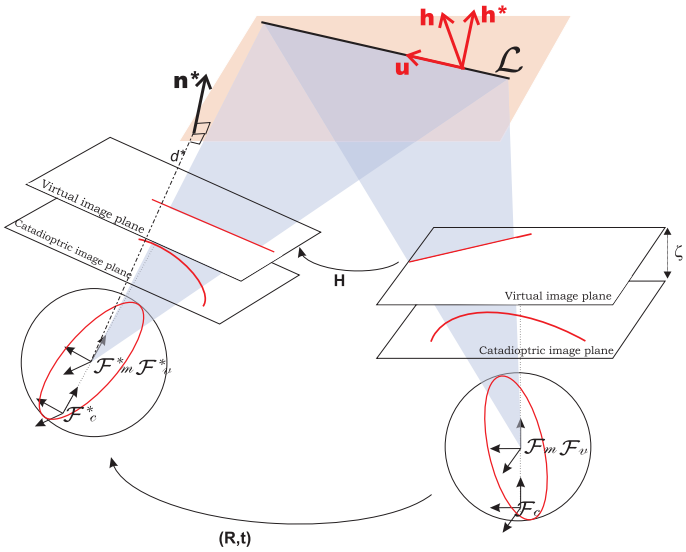

Fig. 2. Motion and structure parameters

the fundamental matrix [15] in pixel space or on the estimation of the essential matrix [14] in normalized space. However, for control purposes, the methods based on the essential matrix are not well suited since degenerate configurations (such as pure rotational motion) can induce unstable behavior of the control scheme. Homography matrix and Essential matrix based approaches do not share the same degenerate configurations, for example pure rotational motion is not a degenerate configuration when using homography-based method. To design a control scheme based on partial Euclidean reconstruction, it is thus preferable to use Homography-based approaches.

The epipolar geometry of central catadioptric system has been more recently investigated (refer for example [11]). The central catadioptric fundamental and essential matrices share similar degenerate configurations that those observed with conventional perspective cameras. In [12], geometrical relationships between two calibrated omnidirectional views of co-planar points have been derived from the non-linear central catadioptric projection model. In the sequel, we show how we can compute homographic relationships between two uncalibrated central catadioptric views knowing only the principal point and using polar lines.

Let $\mathbf{R}$ and $\mathbf{t}$ be the rotation matrix and the translation vector between two positions $\mathcal{F}_m$ and $\mathcal{F}^*_m$ of the central catadioptric camera (see Figure 2). Note that the associate virtual cameras are related by the same motion $(\mathbf{R}, \mathbf{t})$. Let $\mathcal{L}$ be a 3D straight line with binormalized Euclidean Plücker coordinates $[\bar{\mathbf{u}}^\top \ \bar{\mathbf{h}}^\top \ h]^\top$ with respect to $\mathcal{F}_m$ and with coordinates $[\bar{\mathbf{u}}^{*\top} \ \bar{\mathbf{h}}^{*\top} \ h^*]^\top$ with respect to $\mathcal{F}^*_m$. Consider that the 3D line $\mathcal{L}$ lies in a 3D reference plane (π) defined by $\pi^* = [\bar{\mathbf{n}}^{*\top} \ -d^*]$, where $\bar{\mathbf{n}}^*$ is its unitary normal in $\mathcal{F}^*_m$ and d^* is the distance from (π) to the origin of $\mathcal{F}^*_m$. Note that any world point $\mathcal{X} \in \pi$ with coordinates $\mathbf{X} = [X \ Y \ Z]^T$ with respect to $\mathcal{F}_m$ and with coordinates $\mathbf{X}^* = [X^* \ Y^* \ Z^*]^T$ with respect to $\mathcal{F}^*_m$ is projected on the unitary sphere onto the points $\mathbf{X_m} = \mathbf{X}/\|\mathbf{X}\|$ and $\mathbf{X^*_m} = \mathbf{X}^*/\|\mathbf{X}^*\|$ for the two camera positions. The relation between the two projections on the unitary sphere is given by [12]:

$$\mathbf{X_m} \propto \mathbf{H}\mathbf{X^*_m} \tag{6}$$

where $\mathbf{H}$ is a 3×3 homography matrix.

Let $\mathcal{X}_1$ and $\mathcal{X}_2$ be two points in the 3-D space lying on the line $\mathcal{L}$. The central catadioptric projection of the 3-D line $\mathcal{L}$ is fully defined by the normal vector to the interpretation plane $\bar{\mathbf{h}}$. The vector $\bar{\mathbf{h}}$ can be defined by two points in the 3-D line as $\bar{\mathbf{h}} = \frac{\mathbf{X_1} \times \mathbf{X_2}}{\|\mathbf{X_1} \times \mathbf{X_2}\|}$. Noticing that $[\mathbf{H}\mathbf{X}^*_\mathbf{1}]_\times = det(\mathbf{H})\mathbf{H}^{-\top}[\mathbf{X}^*_\mathbf{1}]_\times\mathbf{H}^{-\mathbf{1}}$ ($[\mathbf{H}\mathbf{X}^*_\mathbf{1}]_\times$ being the skew-symetric matrix associated to the vector $\mathbf{H}\mathbf{X}^*_\mathbf{1}$) and according to (6), $\bar{\mathbf{h}}$ can be written as:

$$\bar{\mathbf{h}} \propto \frac{\det(\mathbf{H})}{\|\mathbf{X}^*_\mathbf{1} \times \mathbf{X}^*_\mathbf{2}\|}\mathbf{H}^{-\top}(\mathbf{X_1}^* \times \mathbf{X_2}^*)$$

since $\bar{\mathbf{h}}^* = \frac{\mathbf{X}^*_\mathbf{1} \times \mathbf{X}^*_\mathbf{2}}{\|\mathbf{X}^*_\mathbf{1} \times \mathbf{X}^*_\mathbf{2}\|}$ is the normal vector to the interpretation plane expressed in the frame $\mathcal{F}^*_m$. The relationship beetwen two views of the 3D line can be written by:

$$\bar{\mathbf{h}} \propto \mathbf{H}^{-\top}\bar{\mathbf{h}}^* \tag{7}$$

The expression of the homography matrix in the pixel space can be derived hence using the polar lines. As depicted below, each conic, corresponding to the projection of a 3D line in the omnidirectional image, can be explored through its polar line. Let $\mathbf{l_i}$ and $\mathbf{l^*_i}$ be the polar lines of the image center $\mathbf{O_i}$ with respect to the conics $\mathbf{\Omega_i}$ and $\mathbf{\Omega^*_i}$ respectively in the two positions $\mathcal{F}_m$ and $\mathcal{F}^*_m$ of the catadioptric camera. From equation (4), the relationship given in equation (7) can be rewritten as:

$$\mathbf{l_i} \propto \mathbf{G}^{-\top}\mathbf{l^*_i} \tag{8}$$

where $\mathbf{G} = \mathbf{K}\mathbf{H}\mathbf{K}^{-1}$. Since the polar lines are the perspective projections of the 3D lines in the virtual camera, the homography matrix $\mathbf{G}$ can be decomposed into a rotation matrix and a rank 1 matrix as $\mathbf{G} = \mathbf{K}(\mathbf{R} + \frac{\mathbf{t}}{d^*}\mathbf{n}^{*T})\mathbf{K^{-1}}$. From (8), it is trivial to see that the homography matrix $\mathbf{G}$ related to (π) can be linearly estimated knowing at least four couples of coordinates $((\mathbf{l_i}_k, \mathbf{l^*_i}_k), k = 1 \dots 4)$. From the estimated homography matrix, the camera motion parameters $\mathbf{R}$, $\mathbf{t}^*_d = \frac{\mathbf{t}}{d^*}$ and the structure of the observed scene (for example the vector $\mathbf{n}^*$) can be determined (refer to [10], [23]). It can also be shown that the ratio $\frac{h}{h^*}$ (ratio of the lines depth) can be computed as follow:

$$r = \frac{h}{h^*} = r'\frac{\|\mathbf{n}^* \times \mathbf{K}^\top\mathbf{l^*_i}\|}{\|\mathbf{R}\mathbf{n}^* \times \mathbf{K}^\top\mathbf{l_i}\|} \tag{9}$$

where $r' = \frac{d}{d^*} = 1 + \mathbf{t}^{*\top}_d\mathbf{R}^\top\mathbf{n}^*$.

These parameters are important since they are used in the design of our control scheme. In the next section, we propose a vision control scheme which allows to fully decouple rotational motions from translational motions.

IV. CONTROL SCHEME

In order to design an hybrid visual servoing scheme, the features used as input of the control law combine 2D and 3D information. We propose to derive this information from the polar lines and the homography matrix computed and decomposed as depicted in the last section. Let us first define the input of the proposed hybrid control scheme as follow :

$$\mathbf{s} = [\mathbf{s}_v^\top \;\; \mathbf{s}_\omega^\top]^\top \tag{10}$$

whith $\mathbf{s}_v = [\log(h_1)\ \log(h_2)\ \log(h_3)]^\top$ where h_1, h_2 and h_3 are the depth of three co-planar lines. As we will see in the sequel, by choosing such a feature, the resulting control law allow us to decouple rotational motions from translational motions. The vector $\mathbf{s}_\omega$ is chosen as $\mathbf{s}_\omega = \theta\mathbf{u}^\top$ where $\mathbf{u}$ and θ are respectively the axis and the rotation angle extracted from $\mathbf{R}$ (*i.e* the rotation matrix between the mirror frame when the camera is in the current and desired positions). The task function $\mathbf{e}$ to regulate to 0 is then given by:

$$\mathbf{e} = [\mathbf{s} - \mathbf{s}^*] = [\gamma_1\ \gamma_2\ \gamma_3\ \theta\mathbf{u}^\top]^\top \tag{11}$$

where $\mathbf{s}^* = [\mathbf{s}_v^{*\top}\ \mathbf{0_{1\times 3}}]^\top$ is the desired value of $\mathbf{s}$ and $\gamma_k = \log(h_k/h_k^*)$, for $k = 1\dots 3$. Note that the task function can be directely computed from the estimated homography matrix (γ_k is computed using equation (9) and the rotational part is estimated using partial Euclidean reconstruction from the homography matrix derived in Section III). The exponential convergence of $\mathbf{e}$ can be obtained by imposing $\dot{\mathbf{e}} = -\lambda\mathbf{e}$, the corresponding control law being:

$$\boldsymbol{\tau} = -\lambda\mathbf{L}^{-1}(\mathbf{s} - \mathbf{s}^*) \tag{12}$$

where $\boldsymbol{\tau} = [\mathbf{v}^\top\ \boldsymbol{\omega}^\top]^\top$ is the central catadioptric camera velocity ($\mathbf{v}$ and ω denote respectively the linear and angular velocities). λ tunes the convergence rate and $\mathbf{L}$ is the interaction matrix which links the variation of feature vector $\mathbf{s}$ to the camera velocity ($\dot{\mathbf{s}} = \mathbf{L}\boldsymbol{\tau}$) which we derive now.

The time derivative of $\mathbf{u}\theta$ can be expressed as a function of the camera velocity as:

$$\frac{d(\mathbf{u}\theta)}{dt} = [\mathbf{0_3} \quad \mathbf{L}_\omega]\,\boldsymbol{\tau}$$

$\mathbf{L}_\omega$ is given in [16] by:

$$\mathbf{L}_\omega(\mathbf{u},\theta) = \mathbf{I_3} - \frac{\theta}{2}[\mathbf{u}]_\times + \left(1 - \frac{\mathrm{sinc}(\theta)}{\mathrm{sinc}^2(\frac{\theta}{2})}\right)[\mathbf{u}]_\times^2 \tag{13}$$

where $\mathrm{sinc}(\theta) = \frac{\sin(\theta)}{\theta}$ and $[\mathbf{u}]_\times$ being the skew-symmetric matrix associated to the rotation axis $\mathbf{u}$.

The 3 translational degrees of freedom are controled using the visual observations $\mathbf{s}_v$. From the time derivative of the line depth h_k expressed as a function of the camera velocity [1] given by $\dot{h}_k = (\bar{\mathbf{u}}_\mathbf{k} \times \bar{\mathbf{h}}_\mathbf{k})^\top\mathbf{v}$, it can be shown that:

$$\frac{d(\log(h_k))}{dt} = \left[\tfrac{1}{h_k}(\bar{\mathbf{u}}_\mathbf{k} \times \bar{\mathbf{h}}_\mathbf{k})^\top \quad \mathbf{0_{1\times 3}}\right]\boldsymbol{\tau} \tag{14}$$

From equation (9), it can be shown that $h_k = r_k h_k^*$ and according to (5) and (14), the time derivative of the vector $\mathbf{s}_v$ is thus given by:

$$\dot{\mathbf{s}}_v = [\mathbf{L}_v \quad \mathbf{0_3}]\,\boldsymbol{\tau}$$

where:

$$\mathbf{L}_v = \begin{bmatrix} \|\mathbf{K}^\top\mathbf{l_{i1}}\|r_1h_1^* & 0 & 0 \\ 0 & \|\mathbf{K}^\top\mathbf{l_{i2}}\|r_2h_2^* & 0 \\ 0 & 0 & \|\mathbf{K}^\top\mathbf{l_{i3}}\|r_3h_3^* \end{bmatrix}^{-1} \begin{bmatrix} (\bar{\mathbf{u}}_\mathbf{1}\times\mathbf{K}^\top\mathbf{l_{i1}})^\top \\ (\bar{\mathbf{u}}_\mathbf{2}\times\mathbf{K}^\top\mathbf{l_{i2}})^\top \\ (\bar{\mathbf{u}}_\mathbf{3}\times\mathbf{K}^\top\mathbf{l_{i3}})^\top \end{bmatrix} \tag{15}$$

Once again, note that the time derivative of $\mathbf{s}_v$ does not depend of the camera angular velocity. It is also clear that $\mathbf{L}_v$ is singular only if the principal point M of the mirror frame lies in the 3D reference plane (π). The task function $\mathbf{e}$ can thus be regulated to zero using the control law (12) with the following square block-diagonal interaction matrix:

$$\mathbf{L} = \begin{bmatrix} \mathbf{L}_v & \mathbf{0_3} \\ \mathbf{0_3} & \mathbf{L}_\omega \end{bmatrix} \tag{16}$$

As can be seen on equation (15), the unknown depth h_i^* and the unitary orientations $\mathbf{u}_i$ with respect to the catadioptric camera frame have to be introduced in the interaction matrix. Noticing that $\bar{\mathbf{u}}_i = (\bar{\mathbf{h}}_i \times \mathbf{R}\bar{\mathbf{h}}_\mathbf{i}^*)/\|\bar{\mathbf{h}}_\mathbf{i} \times \mathbf{R}\bar{\mathbf{h}}_\mathbf{i}^*\|$ and using equation (4), the orientation can be estimated as follow:

$$\bar{\mathbf{u}} = \frac{\mathbf{K}^\top\mathbf{l_i} \times \mathbf{R}\mathbf{K}^\top\mathbf{l_i^*}}{\|\mathbf{K}^\top\mathbf{l_i} \times \mathbf{R}\mathbf{K}^\top\mathbf{l_i^*}\|}$$

Furthermore, if the camera is calibrated and $\hat{h}_i^*$ is chosen to approximate h_i^*, then it is clear that $\hat{\mathbf{L}}_v^{-1}\mathbf{L}_v$ is a diagonal matrix with $\hat{h}_i^*/h_i^*$ for $i = 1, 2, 3$ as entries. The only point of equilibrium is thus $\mathbf{s}^*$ and the control law is asymptotically stable in the neighborhood of $\mathbf{s}^*$ if $\hat{h}_i^*$ is chosen positive. In practice, an approximated matrix $\widehat{\mathbf{L}^{*\,-1}}$ at the desired position is used to compute the camera velocity vector and the rotational part can be set to $\mathbf{L}_\omega^{-1}\theta\mathbf{u} = \theta\mathbf{u}$ [16]. Finally, The control law is thus given by:

$$\boldsymbol{\tau} = -\lambda \begin{bmatrix} \widehat{\mathbf{L}_v^{*\,-1}} & \mathbf{0} \\ \mathbf{0} & \mathbf{I_3} \end{bmatrix} \begin{bmatrix} \mathbf{s}_v - \mathbf{s}_v^* \\ \theta\mathbf{u} \end{bmatrix} \tag{17}$$

V. RESULTS

A. Computing Homographies with polar lines

1) Catadioptric camera displacement accuracy: In this simulation, we show the effect of the image noise when estimating the rotation and the direction of the translation from polar lines. Two types of catadioptric cameras have been used: a para-catadioptric camera (combining a parabolic mirror and an orthographic lens) and an hyper-catadioptric camera (combining an hyperbolic mirror with a perspective camera). Only results obtained using the para-catadioptric are presented in this paper since similar results are obtained with the hyper-catadioptric camera. The catadioptric camera observes a grid as presented in Figure 5. The real conics corresponding to the projection of 3D lines are first sampled with a step of 10 pixels. Then, a uniform distribution random noise is added to the sampled points in the direction of the normal vector to the real conic curve. The corrupted points

are fitted to get the coefficients of the conic curve and the principal point is estimated using the intersection of the two lines defined by the intersection of three conics [3]. These coefficients are exploited to compute the polar lines with respect to the estimated principal point. Finally, the polar lines are used to linearly compute the homography matrix and the motion parameters. To improve the quality of the estimated homography, it is also possible to use the linear algorithm to initialize a non-linear one. Since our goal is to provide at video rate the input of a vision-based control scheme, we focused on the linear algorithm. We vary the variance of the random noise to assess the quality of the linear estimator. The rotational error is defined by the distance between the real rotation $\mathbf{R}$ and the estimated one $\widehat{\mathbf{R}}$. This distance is defined by the rotational angle α_r of the matrix $\mathbf{R}\widehat{\mathbf{R}}^\top$. The translational error is defined by the angle α_t between the normalized translation vectors $\mathbf{t}/\|\mathbf{t}\|$ and $\widehat{\mathbf{t}}/\|\widehat{\mathbf{t}}\|$. Figures 3(a) and 3(b) show respectively the evolution of the error angles α_r and α_t with respect to the variance of the image noise (in pixel). The square and diamond plots represent respectively the errors of the estimations when using four and seven 3D lines. As depicted in Figures 3(a) and 3(b), the angle errors α_r and α_t are less than $0.03rad$ (2 degrees) for a variance of 2 pixels. These results confirm that the catadioptric camera displacement can be estimated with a good accuracy when observing coplanar 3D lines, and show that only four 3D lines can be used to estimate the camera displacement. In the next section, results obtained with real data confirm this point.

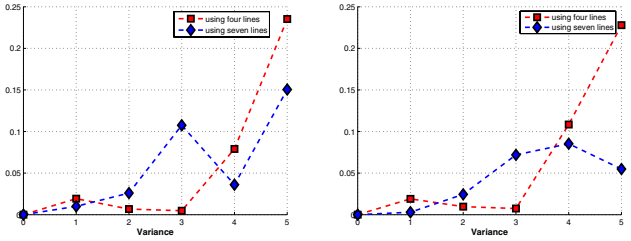

(a) (b)

Fig. 3. Euclidean reconstruction error: (a) error α_r, (b) error α_t

2) Camera displacement from real data: In this experiment, a calibrated para-catadioptric camera is used. The catadioptric camera observes a checkerboard. The conics, corresponding to the 3D lines projection, are extracted using a robust 3D least-square fitting. The camera displacement, from position 1 to position 2, has been set to $\theta\mathbf{u} = [-0.95 \;\; 0.12 \;\; 0.53]^\top$ radian and $\mathbf{t} = [210 \;\; -730 \;\; 490]^\top$ millimeters. Figures 4(a) and 4(b) show respectively the images at positions 1 and 2 and the extracted conics. The associate polar lines with respect to the estimated principal point (yellow cross) are computed and used to estimate the homography matrix and the camera displacement. The rotational and translational angle errors $\alpha_r = 0.025\,rad$ and $\alpha_t = 0.02\,rad$ (as defined above) are very satisfactory since our goal is not to obtain an extremely accurate partial reconstruction but to provide the input of a closed-loop control scheme.

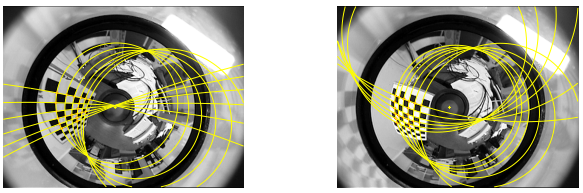

(a) (b)

Fig. 4. Euclidean reconstruction error: (a) image at position 1, (b) image at position 2

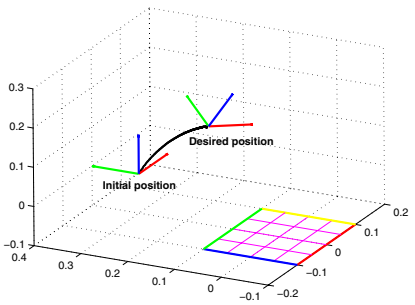

Fig. 5. 3D configuration and camera trajectory of the visual servoing with para-catadioptric camera

B. Visual Servoing

We present now results concerning a positioning task of a six degrees of freedom robotic arm using the previously described control scheme. From an initial position, the catadioptric camera has to reach the desired position. This means that the task function (11), computed from the homography matrix between the current and desired images, converges to zero. To be close to a real setup the observation vector $\mathbf{s}$ is estimated as explained in the previous subsections (the variance of the uniform distribution random noise has been set to 2 pixels). Figure 5 shows the spatial configuration of the 3D lines as well as the 3D trajectory of the central catadioptric camera. The interaction matrix $\mathbf{L}$ is computed using erroneous intrinsic camera parameters (estimated image center and $\pm 10\%$ on the focal length). The value of the interaction matrix $\mathbf{L}$ at the desired position is used to compute the control law (17). The images corresponding to the initial and desired positions are shown by figures 6(c) and 6(d). These figures show the projected 3D lines (conics) and the associated polar lines. The trajectories of the conics and of the corresponding polar lines in the image plane are given in Figures 6(a) and 6(b) respectively. These trajectories confirm that the initial images (conics and polar lines) reach the desired images. Figures 6(e) and 6(f) show respectively the translational and rotational velocities of the catadioptric camera. As shown in Figures 6(g) and 6(h), the error vector $\mathbf{e}$ between the current and desired observation vectors are well regulated to zeros, and thus the positioning task is correctly realized.

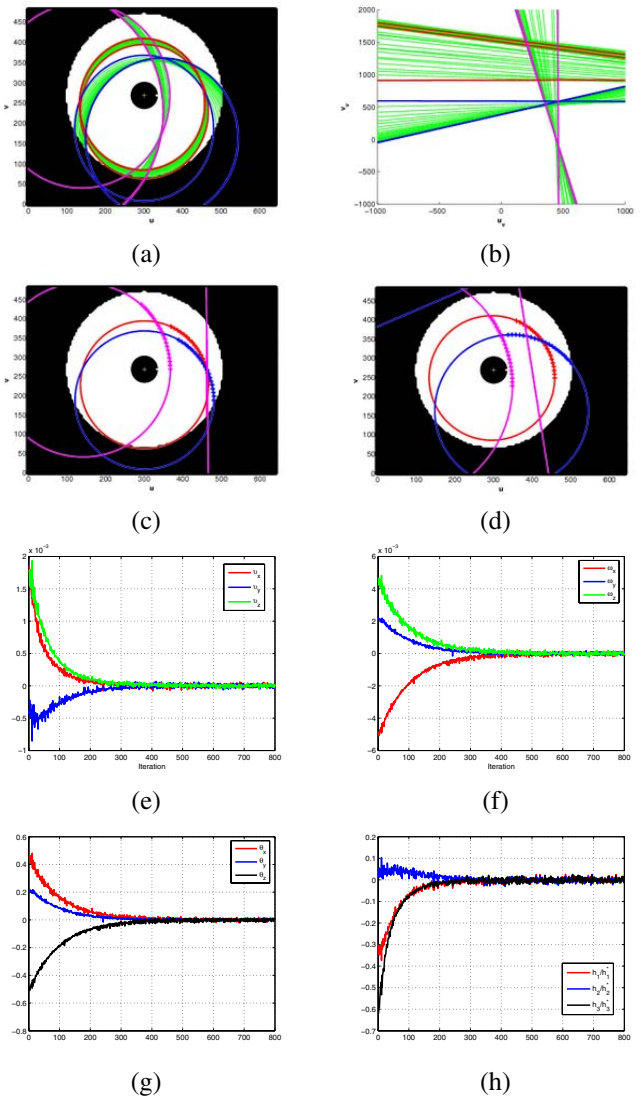

Fig. 6. Visual servoing with para-catadioptric camera: (a) trajectory of the conics in the image plane, (b) trajectory of the polar lines, (c) initial image, (d) desired image, (e) translation velocities [m/s], (f) rotational velocities [rad/s], (g) $\theta\mathbf{u}$ errors, (h) $(\mathbf{s}_\upsilon - \mathbf{s}^*_\upsilon)$ vector errors

VI. Conclusion

In this paper a new hybrid decoupled vision-based control scheme valid for the entire class of central cameras was presented. Geometrical relationship between polar lines and conic curves was exploited to estimate a generic homography matrix from which partial Euclidean reconstruction can be obtained. Results with simulated and real data confirmed the relevance and accuracy of the approach. The information extracted from the homography matrix were then used to design a hybrid control law which allowed us to fully decouple rotational motion from translational motions. In future work, the robustness and stability analysis with respect to calibration errors must be studied.

References

[1] N. Andreff, B. Espiau, and R. Horaud. Visual servoing from lines. *International Journal of Robotics Research*, 21(8):679–700, August 2002.

[2] S. Baker and S. K. Nayar. A theory of single-viewpoint catadioptric image formation. *International Journal of Computer Vision*, 35(2):1–22, November 1999.

[3] J. Barreto and H. Araujo. Geometric properties of central catadioptric line images. In *7th European Conference on Computer Vision, ECCV'02*, pages 237–251, Copenhagen, Denmark, May 2002.

[4] J. P. Barreto, F. Martin, and R. Horaud. Visual servoing/tracking using central catadioptric images. In *ISER2002 - 8th International Symposium on Experimental Robotics*, pages 863–869, Bombay, India, July 2002.

[5] R. Benosman and S. Kang. *Panoramic Vision*. Springer Verlag ISBN 0-387-95111-3, 2000.

[6] P. Blaer and P.K. Allen. Topological mobile robot localization using fast vision techniques. In *IEEE International Conference on Robotics and Automation*, pages 1031–1036, Washington, USA, May 2002.

[7] F. Chaumette. Potential problems of stability and convergence in image-based and position-based visual servoing. *The Confluence of Vision and Control, D. Kriegman, G. Hager, A. Morse (eds), LNCIS Series, Springer Verlag*, 237:66–78, 1998.

[8] G. Chesi, K. Hashimoto, D. Prattichizzo, and A. Vicino. A switching control law for keeping features in the field of view in eye-in-hand visual servoing. In *IEEE International Conference on Robotics and Automation*, pages 3929–3934, Taipei, Taiwan, September 2003.

[9] Noah J. Cowan, Joel D. Weingarten, and Daniel E. Koditschek. Visual servoing via navigation functions. *IEEE Transactions on Robotics and Automation*, 18(4):521–533, August 2002.

[10] O. Faugeras and F. Lustman. Motion and structure from motion in a piecewise planar environment. *Int. Journal of Pattern Recognition and Artificial Intelligence*, 2(3):485–508, 1988.

[11] C. Geyer and K. Daniilidis. Mirrors in motion: Epipolar geometry and motion estimation. In *International Conference on Computer Vision, ICCV03*, pages 766–773, Nice, France, 2003.

[12] H. Hadj Abdelkader, Y. Mezouar, N. Andreff, and P. Martinet. 2 1/2 d visual servoing with central catadioptric cameras. In *IEEE/RSJ Int. Conf. on Intelligent Robots and Systems, IROS'05*, pages 2342–2347, Edmonton, Canada, August 2005.

[13] S. Hutchinson, G.D. Hager, and P.I. Corke. A tutorial on visual servo control. *IEEE Transactions on Robotics and Automation*, 12(5):651–670, October 1996.

[14] H.C. Longuet-Higgins. A computer algorithm for reconstructing a scene from two projections. *Nature*, 293:133–135, September 1981.

[15] Quang-Tuan Luong and Olivier Faugeras. The fundamental matrix: theory, algorithms, and stability analysis. *Int. Journal of Computer Vision*, 17(1):43–76, 1996.

[16] E. Malis, F. Chaumette, and S. Boudet. 2 1/2 d visual servoing. *IEEE Transactions on Robotics and Automation*, 15(2):238–250, April 1999.

[17] Y. Mezouar and F. Chaumette. Path planning for robust image-based control. *IEEE Transactions on Robotics and Automation*, 18(4):534–549, August 2002.

[18] Y. Mezouar, H. Haj Abdelkader, P. Martinet, and F. Chaumette. Central catadioptric visual servoing from 3d straight lines. In *IEEE/RSJ Int. Conf. on Intelligent Robots and Systems, IROS'04*, volume 1, pages 343–349, Sendai, Japan, September 2004.

[19] A. Paulino and H. Araujo. Multiple robots in geometric formation: Control structure and sensing. In *International Symposium on Intelligent Robotic Systems*, pages 103–112, University of Reading, UK, July 2000.

[20] E. Malis S. Benhimane. Vision-based control with respect to planar and non-planar objects using a zooming camera. In *IEEE International Conference on Advanced Robotics*, pages 863–869, July 2003.

[21] R. Vidal, O. Shakernia, and S. Sastry. Formation control of nonholonomic mobile robots with omnidirectional visual servoing and motion segmentation. In *IEEE International Conference on Robotics and Automation*, pages 584–589, Taipei, Taiwan, September 2003.

[22] N. Winter, J. Gaspar, G. Lacey, and J. Santos-Victor. Omnidirectional vision for robot navigation. In *Proc. IEEE Workshop on Omnidirectional Vision, OMNIVIS*, pages 21–28, South Carolina, USA, June 2000.

[23] Z. Zhang and A. R. Hanson. Scaled euclidean 3d reconstruction based on externally uncalibrated cameras. In *IEEE Symposium on Computer Vision*, Coral Gables, FL, 1995.